Heliyon 10 (2024) e35792

Contents lists available at ScienceDirect

Heliyon

journal homepage: www.cell.com/heliyon

Research article

Dynamic weighted residual ensemble learning for hyperspectral image classification driven by features and samples

Jing Wang [a,*], Guoguo Yang [a], Hongliang Lu [b,c]

[a] Department of Geographic Information and Tourism, Chuzhou University, Chuzhou, 239000, China
[b] School of Earth Sciences and Engineering, Hohai University, Jiangning, Nanjing, 211100, China
[c] School of Architectural Engineering, Tongling University, Tongling, 244000, China

ARTICLE INFO

Keywords:
Dynamic ensemble selection
Multi-feature
Bootstrap
Residual ensemble learning
Hyperspectral imagery

ABSTRACT

Dynamic ensemble selection has emerged as a promising approach for hyperspectral image classification. However, selecting relevant features and informative samples remains a pressing challenge. To address this issue, we introduce two novel dynamic residual ensemble learning methods. The first proposed method is called multi-features driven dynamic weighted residuals ensemble learning (MF-DWRL). This method leverages various combinations of features to construct classifier pools that incorporate feature differences. The K-Nearest Neighbors algorithm is employed to establish the region of competence (RoC) in the dynamic ensemble selection process. By assessing the performance of the RoC, the feature sets that yield the highest classification accuracy are identified as the optimal feature combinations. Additionally, the classification accuracy is utilized as prior information to guide the residual adjustments of each classifier. The second method, known as features and samples double-driven dynamic weighted residual ensemble learning (FS-DWRL), further enhances the performance of the ensemble. This approach not only considers the selection of feature combinations but also takes into account the informative samples. By jointly optimizing the feature and sample selection processes, FS-DWRL achieves superior classification accuracy compared to existing state-of-the-art methods. To evaluate the effectiveness of the proposed methods, three hyperspectral datasets from China—WHU-Hi-HanChuan, WHU-Hi-LongKou, and WHU-Hi-HongHu—are used for classification experiments. For these datasets, the proposed methods achieve the highest classification accuracies of 90.57 %, 98.77 %, and 91.08 %, respectively. The MF-DWRL and FS-DWRL methods exhibit significant improvements in classification accuracy.

1. Introduction

Hyperspectral imaging (HSI) contains extensive spectral information with hundreds of contiguous spectral bands [1,2], enabling its wide application in various fields such as geoscience [3], biomedicine [4], agriculture [5], geological prospecting [6], and environmental studies [7]. However, HSI classification faces challenges, including redundancy, high dimensionality, and a scarcity of labeled samples [8–14]. To address these issues, advanced technologies such as deep learning and ensemble learning strategies have been developed.

* Corresponding author.
E-mail address: wangjing@chzu.edu.cn (J. Wang).

https://doi.org/10.1016/j.heliyon.2024.e35792
Received 24 July 2023; Received in revised form 2 August 2024; Accepted 2 August 2024
Available online 5 August 2024

Active learning [15,16], as a deep learning method, allows the model to proactively select samples it deems most informative for labeling, thereby serving for training. This is especially crucial for hyperspectral images, which require extensive annotation costs. The essence of this approach is that the model actively chooses data samples that are most beneficial for its training, thus reducing the need for manual labeling, especially in the expensive annotation realm of hyperspectral imaging. When applying deep learning models, such as Convolutional Neural Networks (CNNs) [17], to HSI classification, integrating active learning can more precisely select key samples. This not only enhances the model's classification accuracy but also effectively reduces training costs and time. Mainstream active learning strategies primarily include uncertainty-based sampling, which chooses samples where the model's prediction is most uncertain; representativeness-based sampling, which emphasizes selecting samples that can represent a large portion of unlabeled data; and model-improvement strategies, which opt for samples most likely to enhance model performance [18–20]. In summary, active learning offers an effective means of reducing annotation costs and boosting model performance in hyperspectral image classification. However, despite its commitment to minimizing labeling requirements, active learning might be affected by model bias, limitations in data selection, ongoing annotation costs, data imbalance, and scope of its application [21]. Ensemble learning [22], by combining multiple models, can balance out these biases, strengthen model generalization, and doesn't rely on continuous user annotation. It is also better equipped to handle data imbalances and showcases broader adaptability. Hence, compared to active learning, ensemble learning exhibits clear advantages in various aspects.

Firstly, hyperspectral data often contains redundant information because neighboring pixels in an image are likely to have similar spectral signatures. This redundancy can lead to inefficiencies in classification algorithms. Ensemble learning can help by combining multiple classifiers, each trained on a subset of the data or with different features, reducing the impact of redundancy. By aggregating the results of multiple classifiers, ensemble methods can capture a broader range of information and reduce the influence of redundant data. Secondly, hyperspectral data is characterized by a high number of spectral bands, resulting in high-dimensional feature spaces. High dimensionality can lead to increased computational complexity and overfitting. Ensemble learning can mitigate this by using techniques such as feature selection or dimensionality reduction in combination with individual classifiers. By reducing the dimensionality of the data before classification, ensemble methods can improve the efficiency and effectiveness of the classification process. Lastly, HSI classification often suffers from a lack of labeled training samples, making it challenging to train accurate classifiers. Ensemble learning can address this limitation by allowing the integration of weak or limited classifiers. It combines the predictions of multiple classifiers to make a final decision, enhancing overall classification performance even with few labeled samples. Some ensemble techniques [22], like bootstrapping and bagging, can generate multiple subsets of the available labeled data to train diverse classifiers, which can be particularly useful when data is limited. In summary, ensemble learning strategies can help improve HSI classification by leveraging multiple classifiers to handle redundancy, reduce dimensionality, and make the most of the available labeled data. By combining the strengths of multiple classifiers, ensemble methods aim to enhance classification accuracy and robustness in scenarios where traditional single classifiers may struggle due to the mentioned limitations.

Ensemble learning models can be mainly divided into two categories: static ensemble methods and dynamic ensemble selection (DES) methods. The static ensemble method [23] is based on the idea that a weak classifier can be promoted to a strong classifier through a specific ensemble strategy. Classic methods include bagging and boosting. In the bagging method [24,25], a diverse classifier pool is generated using the bootstrap strategy. Better classification results are then obtained based on the classifiers in the pool through a specific fusion strategy. Boosting [26–28] promotes a weak classifier to a strong classifier by weighting the samples, reducing variance and bias. Zhang et al. [29] proposed a new ensemble learning method based on sparse joint representation, incorporating both spectral and spatial features of hyperspectral data. The results show that the proposed method can perform better than traditional ensemble methods. Li et al. [30] proposed a new ensemble network for hyperspectral object tracking, which demonstrates effectiveness and better performance compared to other models. Su et al. [31] proposed a new ensemble learning framework using the tangent collaborative representation model as the base classifier, showing that representation models can also be used in ensemble learning. However, the static ensemble method does not consider each classifier's specific classification effects on different targets, and the accuracy of prior information for the base classification is difficult to obtain. The second category is the dynamic ensemble selection (DES) method [32–35]. This method first uses K-NN or clustering to divide the classification targets into different regions, called regions of competence (RoC), and then selects the best classifier set for each local target according to some evaluation indicators. DES can better utilize the regional advantage of each base classifier compared to the static ensemble method. Even a less capable classifier may perform better in a local area. The purpose of DES is to leverage the unique classification advantages of each classifier [36–38]. Bharath and Rama [39] applied the idea of dynamic classifier selection (DCS) to hyperspectral image classification, combining dimensionality reduction and dynamic selection to construct a new DCS strategy. Meanwhile, Bharath et al. [40] proposed a DES method for heterogeneous classifiers, using the Markov random field (MRF), extreme learning machine (ELM), and random subspace method (RSM) as base classifiers. The results show that the dynamic classifier selection method can be effectively applied to HSI classification. Additionally, Lu et al. [41] proposed a new RoC construction method based on multi-view clustering for DES, which shows better classification accuracy than traditional DES models. However, current DES methods are limited to selecting classifiers without considering the adaptability of different samples and features to the target area. In summary, the static ensemble method can better utilize the advantages of different classifiers, but it often ignores the specific classification performance of multiple classifiers for different targets. Without prior selection of classifiers, the performance of classifier ensembles may be lower than that of a single classifier. Although the DES method focuses on the classifier's behavior, it does not consider the impact of features and samples on the classification target.

Therefore, this paper proposes a hyperspectral image classification strategy based on a diversity-guided dynamic sample and feature selection method. The research introduces a novel dynamic ensemble feature selection method for hyperspectral remote sensing image analysis, utilizing heterogeneous collaborative representation classification. Additionally, it presents a strategy that

combines dynamic feature and sample selection to address the issue of insufficient sample information in existing classification methods through bootstrap sampling. Finally, a weighted residual ensemble framework is proposed, leveraging the prior behaviors of classifiers obtained from previous methods for residual-weighted ensemble, aiming to achieve more accurate classification results. The main contributions of the paper are as follows:

1) In response to the lack of exploration of hyperspectral remote sensing image features in existing dynamic ensemble learning methods, a dynamic ensemble feature selection method based on heterogeneous collaborative representation classification is proposed in this paper for the first time. The K-NN method is used to construct a validation set to obtain priori information. Then, according to a certain accuracy measurement metrics, a feature or a feature set with higher classification accuracy is selected for HSI classification, which can better exploit the local classification advantages of each feature. Compared to traditional methods, the proposed approach introduces, for the first time, dynamic ensemble theory-based feature selection, which can more fully exploit the local classification advantages of each feature while simultaneously improving computational efficiency while ensuring classification accuracy.
2) To address the issue of inadequate exploration of sample information in existing hyperspectral remote sensing image classification, this paper proposes a strategy that combines dynamic feature and sample selection using bootstrap sampling based on the concept of dynamic selection. In contrast to traditional classification methods that use all samples for classification, this paper utilizes the RoC obtained in advance from dynamic ensembles to acquire prior information about the samples. Consequently, samples with higher confidence are selected for classification, providing better training samples and further enhancing classification accuracy.
3) A weighted residual ensemble framework is proposed in the paper. Unlike traditional ensemble learning methods, the classifier prior behavior obtained in 1) and 2) is utilized to directly perform a weighted ensemble with the residuals of the collaborative classifiers. According to the differences of multiple CR-based classifier sets, the method constrains the residuals of the classifiers by their prior behaviors, so as to obtain weighted classification results.

The remainder of this paper is organized as follows. In Section 2, the proposed FS-DWRS and MF-DWRL are presented. The results of the experiment are demonstrated in Section 3. In Section 4, the robustness, extensibility, transferability, and convergence of the proposed algorithms are discussed in detail. Finally, the conclusions of this study are drawn in Section 5.

2. methodology

2.1. Related works

2.1.1. Kernel collaborative representation classifiers (KCRC)

The basic idea of collaborative representation [42–45] is to indicate the data measurement data with the least samples. Given a training set $\boldsymbol{X} = [\boldsymbol{x_1}, .., \boldsymbol{x_n}] \in \boldsymbol{R^{m \times n}}$ for $\boldsymbol{n}$ classes, a test sample $\in \boldsymbol{R^m}$. The target is to solve the l_2 minimization problem.

$$\widehat{\boldsymbol{x}}_{\boldsymbol{1}} = \underset{\boldsymbol{x}}{\operatorname{argmin}} \|\boldsymbol{x}\|_2 subjectto \|\boldsymbol{\alpha X} - \boldsymbol{y}\|_2 < \varepsilon \tag{1}$$

where $\boldsymbol{\alpha}$ is the representation coefficient. Compute the residuals.

$$\boldsymbol{r}_i(\boldsymbol{y}) = \|\boldsymbol{y} - \boldsymbol{\alpha x}_i\|_2, for\ i = 1, \ldots, n \tag{2}$$

where n represents the number of classes. Finally, sample $\boldsymbol{y}$ can be classified as.

$$class(\boldsymbol{y}) = \underset{i}{\operatorname{argmin}} \boldsymbol{r}_i(\boldsymbol{y}) \tag{3}$$

Meanwhile, to solve the problem of standard linearity, some studies have proposed an algorithm with kernel tricks, which is the KCRC [45] model. However, the residuals of KCRCs with different parameters are quite disparate. Therefore, a new weighted residual ensemble method to get more reliable classifier results is proposed in the paper.

2.1.2. Dynamic ensemble selection

Dynamic ensemble selection (DES) is a classifier selection strategy that can assign one or some classifiers with optimal competence for a specific test region. The basic idea of the DES method is that each weak classifier has its own unique classification advantages for predicting a particular region of the target. Therefore, the validation data and test data into regions with homogeneity, and uses the classification accuracy of the classifier on the validation set as the prior information in DES. Then the optimal classifier or classifier set is assigned to the target region. Finally, the final results are obtained by these regions which are ca lled region of competence (RoC). The processes of DES can be divided into three steps:

Similar to traditional methods, DES method also needs to obtain a classifier pool with diversity. The diversity of classifiers can be often obtained by setting different features, selecting different types of models, or using different training data (different samples, multiple features).

The clustering and K-NN methods are standard techniques for defining regions of competence (RoC) in dynamic ensemble selection (DES). The fundamental idea is to exploit the correlation between validation and test data. Specifically, the connection between labeled samples (test samples) and unlabeled samples (validation samples) is established through specific metrics. By partitioning

them into the same regions and creating connections between unknown samples and labeled samples, the sample space is divided into several regions. Selecting well-performing base classifiers within each region enhances the classification performance and generalization ability of the ensemble model. In the K-NN method, *k* samples around each test point are obtained by calculating the distance between samples. These samples are then used as a validation set to provide prior information for each classifier. Based on the RoC constructed as described, the optimal classifier or classifier set is assigned to each capability area using specific evaluation indicators and selection methods. Finally, a voting method is employed to obtain the final classification result.

2.2. Proposed methods

2.2.1. Multi-features driven dynamic weighted residuals ensemble learning (MF-DWRL)

Algorithm 1 MF-DWRL

Input: Multiple feature combinations data set $\mathbf{X_f}$; the **k** value; the empty ensemble of features $\boldsymbol{EoF_t}$; testing samples **y**
for each testing sample **t** in **do**
  Obtain $\mathbf{\Psi_{te}}$ as the K region of competence by K-NN based on validation set
  for each classifier $\mathbf{c_i}$ generation by feature combinations in $\mathbf{X_f}$ **do**
  1. Calculating the residuals of each $\mathbf{c_i}$ according to Eqs. (5)–(9);
  2. Obtaining the classification accuracy **OA** and weights matrices **w** of each $\mathbf{c_i}$ according to Eq. (10)–(12);
3. Using the classification accuracy in step.2 to screen the two best feature combinations as the best training features;
4. Getting the final weighted residuals fusion results **WR** according to Eq. (13)
  end for
  Use the ensemble EoF^*_t to classify testing set according to Eq. (14)
end for
Output: class(y)

The process of the two proposed algorithms is mainly divided into three parts: pool generation, weight matrices and accuracy calculating, dynamic residuals selection and fusion. The structure of two methods is shown in Fig. 1.

1) Classifier pool generation by multi-features

Three different features are used as input for the classifier pool: spectral features, Extend Morphological Profile (EMP) features, and Gabor features. In order to measure the influence of different features on the classification accuracy of hyperspectral images, the base classifiers with multiple features combination are constructed in the paper. It is mainly divided into three combinations: single feature,

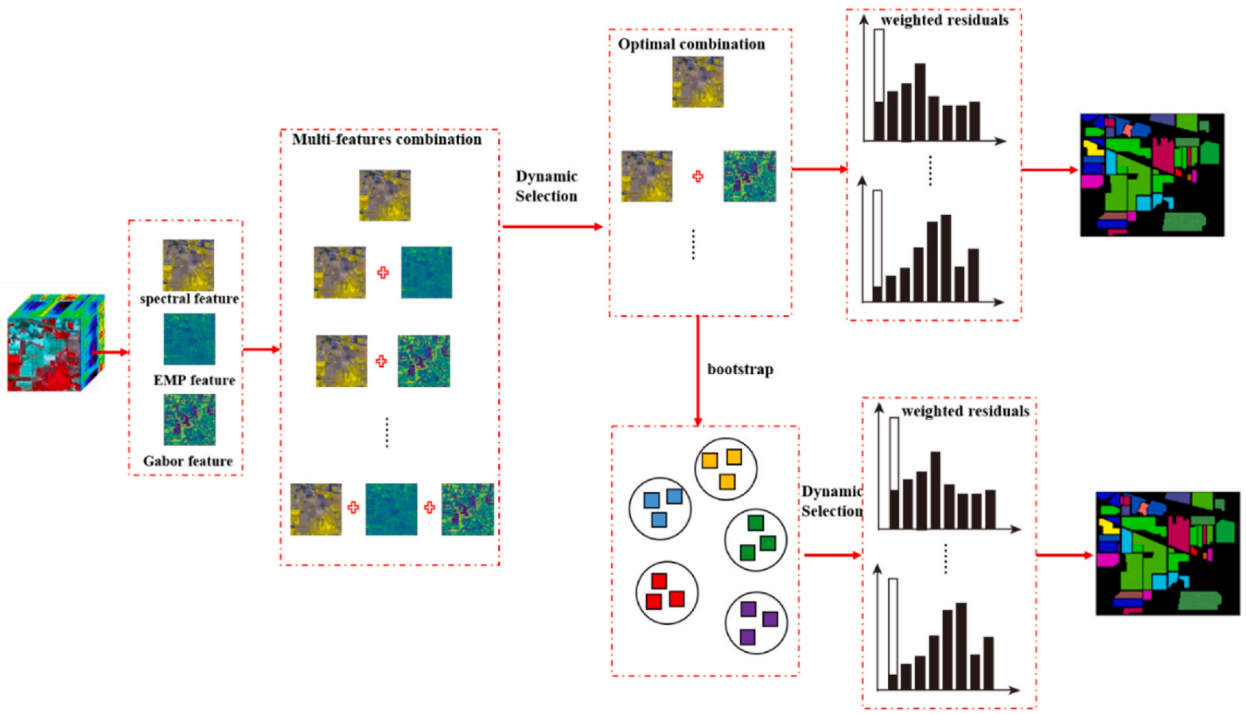

Fig. 1. Flowchart of proposed methods.

double features, and multi-features. They are denoted as

$$\boldsymbol{X}_f = \left[\boldsymbol{x}_f{}^1, \ldots, \boldsymbol{x}_f{}^m\right] \tag{4}$$

where $\boldsymbol{x}_f{}^m$ is different combinations of multiple features, and m represents the number of features.

Unlike traditional methods, in order to make the algorithms more focus on feature selection, only the kernel collaborative representation classifier (KCRC) as the base classifier for the construction of the classifier pool. At last, the pool with multiple classifiers is denoted as $\boldsymbol{F} = \{\boldsymbol{f}_1, \boldsymbol{f}_2, \ldots, \boldsymbol{f}_c\}$, where c represents the number of base classifiers.

2) Get residuals and accuracy by K-NN validation samples

Firstly, given a training set $\boldsymbol{X}_{tr}$, according to formula (1), the representation coefficient of multiple features can be obtained by using the classifier $\boldsymbol{f}_i$.

$$\widehat{\boldsymbol{X}}_{tr}^{i} = \underset{x}{\operatorname{argmin}} \left\|\boldsymbol{x}_{tr}^{i}\right\|_2 subject to \left\|\boldsymbol{\alpha}_{tr}^{i}\boldsymbol{X}_{tr}^{i} - \boldsymbol{y}^{i}\right\|_2 < \varepsilon, i = 1, \ldots, c. \tag{5}$$

where $\boldsymbol{x}_{tr}^{i}$ is the training samples of the ith classifier in the pool, and the $\boldsymbol{\alpha}_{tr}^{i}$ is the corresponding representation coefficients which is solved as

$$\boldsymbol{\alpha}_{tr}^{i} = \left(\boldsymbol{X}_{tr}^{i\,T}\boldsymbol{X}_{tr}^{i} + \lambda \boldsymbol{I}\right)^{-1}\boldsymbol{X}_{tr}^{i\,T}\boldsymbol{y}^{i} \tag{6}$$

Then a coefficient matrix of each classifier $\boldsymbol{f}_i$ is obtained, as

$$\boldsymbol{\alpha} = [\boldsymbol{\alpha}_1, \ldots, \boldsymbol{\alpha}_i], i = 1, \ldots, c. \tag{7}$$

Calculating the residual according to formula (2), and obtaining the residual matrix:

$$\boldsymbol{r}(\boldsymbol{y}) = \|\boldsymbol{y} - \boldsymbol{\alpha}\boldsymbol{x}_{tr}\|_2, i = 1, \ldots, c \tag{8}$$

Then the residual matrix is obtained

$$RES = [\boldsymbol{r}_1, \ldots, \boldsymbol{r}_i], i = 1, \ldots, c \tag{9}$$

where RES is the residual matrix of each classifier $\boldsymbol{f}_i$. Then the validation set $\boldsymbol{X}_v = \left[\boldsymbol{x}_v{}^1, \ldots, \boldsymbol{x}_v{}^k\right]$ is obtained by K-NN algorithm. For $\boldsymbol{f}_i$ in the classifier pool, the classification performance in k validation set is obtained, which is denoted as

$$\boldsymbol{X}_v = \left[\boldsymbol{x}_v{}^1, \ldots, \boldsymbol{x}_v{}^k\right] \tag{10}$$

where the $\boldsymbol{OA}_i$ is the overall accuracy of the ith classifier.

2.2.1.1. According to Eq. (4), the weight matrices is calculating

$$\boldsymbol{W} = [\boldsymbol{w}_1, \ldots, \boldsymbol{w}_i] \tag{11}$$

$$\boldsymbol{w}_i = \frac{\boldsymbol{OA}_i}{\sum_{1}^{i} \boldsymbol{OA}_i} \tag{12}$$

where $\boldsymbol{w}_i$ represents the weight of the classification accuracy of the ith classifier in the pool for the validation.

3) Dynamic residuals ensemble selection and fusion

According to Eq. (10), the two sets of feature combinations with the best performance are chosen as the optimal training features, denoted as $\boldsymbol{w}_{b1}$ and $\boldsymbol{w}_{b2}$.

Finally, the weighted residual is obtained by Eq. (4):

$$\boldsymbol{WR} = \boldsymbol{w}_{b1}\boldsymbol{r}_{b1} + \boldsymbol{w}_{b2}\boldsymbol{r}_{b2} \tag{13}$$

where $\boldsymbol{w}_{b1}$ and $\boldsymbol{w}_{b2}$ are the optimal features selected by DES, $\boldsymbol{r}_{b1}$ and $\boldsymbol{r}_{b2}$ are the corresponding residuals. Then the final classification result is obtained according to formula (3):

$$class(\boldsymbol{y}) = \operatorname{argmin}\boldsymbol{WR}(\boldsymbol{y}) \tag{14}$$

2.2.2. Features and samples double driven dynamic weighted residual ensemble learning (FS-DWRL)

Algorithm 2 FS-DWRL

Input: Optimal feature combinations data set $\mathbf{X'_f}$; numbers of resample times N; testing samples $\mathbf{y}$ **for** $\mathbf{X'_f}$ **do**
Use the bootstrap method to sampling X' and get sub training set X'_{sub} for each classifier c_i generation by sub_X_f do
1. Calculating the residuals of each $\mathbf{c_i}$ according to Eq. (15)–(17);
2. Obtaining the classification accuracy **OA** and weights matrices **w** of each $\mathbf{c_i}$ according to Eq. (18) and (19);
3. Getting the final weighted residuals fusion results **WR'** according to Eq. (20)
end for
Classify testing set by $EoF^*{}_t$ according to (21) **end for Output:** class(y)

1) New classifier pool generation by Bootstrap sampling

According to the optimal features $\boldsymbol{X}'_{sub}$ based on MF-DWRL algorithm, the bootstrap is used to resample the training data in into n groups, denoted as

$$\boldsymbol{X}'_{sub} = \left[\boldsymbol{x}'_{sub\ 1}, \ldots, \boldsymbol{x}'_{sub\ q}\right] \tag{15}$$

where $\boldsymbol{x}'_{sub\ i}$ is the sub-training set and q represents the number of subsets. Then the new classifier is constructed based on $\boldsymbol{X}'_{\boldsymbol{sub}}$, which is denoted as

$$\boldsymbol{F}' = \left[\boldsymbol{f}'_1, \ldots, \boldsymbol{f}'_q\right] \tag{16}$$

where $\boldsymbol{F}'$ is the new classifier pool generated based on a sub-training set.

2) Get residuals and weight matrices by K-NN validation samples

Similar to the MF-DWRL, the residual of new classifier pool is calculating as,

$$\boldsymbol{r}(\boldsymbol{y}) = \|\boldsymbol{y} - \boldsymbol{\alpha x}'\|_2, i = 1, \ldots, q \ \ \boldsymbol{RES}' = \left[\boldsymbol{r}'_1, \ldots, \boldsymbol{r}'_q\right] \tag{17}$$

where $\boldsymbol{RES}'$ is the residual matrix of each classifier $\boldsymbol{f}'_{\boldsymbol{i}}$.

The prior accuracy information and weight matrix for each classifier is calculated by validation set using $\boldsymbol{X}_{sub}$, denoted as

$$\boldsymbol{OA} = \left[\boldsymbol{OA}_1, \ldots, \boldsymbol{OA}_q\right] \tag{18}$$

$$\boldsymbol{w}_i = \frac{\boldsymbol{OA}_i}{\sum_{1}^{i} \boldsymbol{OA}_i} \tag{19}$$

where $\boldsymbol{w_i}$ represents the weight of the classification accuracy of the ith classifier in the pool for the validation.

2.2.2.1. Dynamic weighted residuals ensemble learning. Finally, the weighted residual is obtained

Table 1
The WHU-Hi-HanChuan data set.

No.	Samples	Name
1	44735	Strawberry
2	22753	Cowpea
3	10287	Soybean
4	5353	Sorghum
5	1200	Water spinach
6	4533	Watermelon
7	5903	Greens
8	17978	Trees
9	9469	Grass
10	10516	Red roof
11	16911	Gray roof
12	3679	Plastic
13	9116	Bare soil

$$\boldsymbol{WR}' = \sum_{i=1}^{n} \boldsymbol{w}_i' \boldsymbol{r}_i' \tag{20}$$

where $\boldsymbol{WR}'$ is the weighted residuals.

Then the final classification result is obtained

$$class(\boldsymbol{y}) = \text{argmin}\boldsymbol{WR}'(\boldsymbol{y}) \tag{21}$$

3. Results

3.1. Data source

The WHU-Hi-HanChuan data set [46] is the first hyperspectral image to evaluate the proposed methods. It contains 274 spectral bands with the wavelengths ranging from 0.4 to 1 μm, which is obtained by UAV hyperspectral remote sensing observation in Hanchuan, Hubei Province, China. The details of this data are listed in Table 1. The false-color image and ground truth are shown in Fig. 2 (a) and 2 (b).

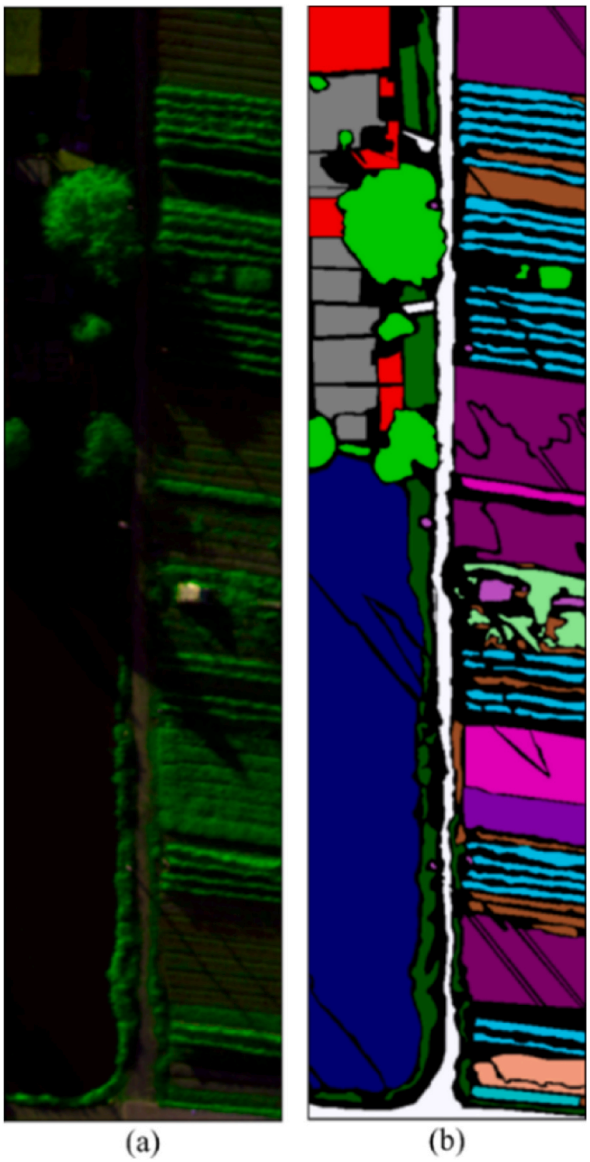

Fig. 2. (a) False-color image and (b) ground truth of the WHU-Hi-HanChuan data set.

The WHU-Hi-LongKou data set [46] contains 270 spectral bands with wavelengths ranging from 0.4 to 1 μm, which is acquired by UAV hyperspectral remote sensing observation in Longkou, Hubei Province, China. The details of nine classes in this HIS are listed in Table 2. The false-color image and ground truth are presented in Fig. 3 (a) and 3 (b).

The WHU-Hi-HongHu data [46] set is gathered by UAV hyperspectral remote sensing observation in Honghu, Hubei Province, China. It contains 270 spectral bands with 940 x 475 pixels. The detailed information of each class is shown in Table 3 and Fig. 4 (a) and 4 (b).

3.2. Experimental setup

All experiments are implemented on the platform of Python 3.8.6. The specific parameters of the proposed algorithms are set as follows.

3.2.1. Parameter setup

The range of k number $\boldsymbol{n\_k}$ in DWR-DEL is set {1, 2, 3, 4, 5}. The number of resample $\boldsymbol{n\_r}$ is set {5, 10, 15, 20, 25}. The regularization parameter λ is set {1e-1, 1e-2, 1e-3, 1e-4, 1e-5}. The data partitioning was conducted using a random sampling approach. Each class was separately sampled with {5, 10, 15, 20, 25} instances for experimentation. The presented results represent the outcomes obtained using 25 samples per class. Additionally, the hyperparameters of different algorithms for all the dataset are set to the same values.

3.2.2. Multi-features construct

To ensure the comparability and fairness, the compared and proposed algorithms are under the same experimental conditions. The classifier pool through different feature combinations, namely Spectral feature (sf), EMP feature (ef), and Gabor feature (gf) is used to evaluate the proposed methods in this paper. To focus on feature and sample selection, only KCRC classifier is used as base classifier in this paper.

3.2.3. Baseline and comparative algorithms

To evaluate the performance of the proposed algorithm, multiple classification algorithms were used for comparison. For example, the classic machine learning algorithms SVM and RF are the baselines. Moreover, the ensemble algorithm GBDT [47], LightGBM [48], and XGboost [49] are also used as a comparison algorithm. In addition, the two advanced DES algorithms, DES-MI [50] and META-DES [51] algorithm are used as comparative algorithms in the paper The overall accuracy (OA), average accuracy (AA), and kappa indexes are used to evaluate the classification of all the comparisons and proposed methods in this section. OA measures the proportion of correctly classified instances over the total, AA considers accuracy for each class and averages them, while the kappa index adjusts accuracy for chance agreement, making it valuable for comparing methods or assessing inter-rater agreement.

3.3. Classification performance and maps

The classification performance of proposed methods and comparative algorithms for the first data set are shown in Table 4. The classification images obtained by these methods are shown in Fig. 5 (a)–(l). For the WHU-Hi-HanChuan data set,

the classification performance of proposed methods is better than other comparative models. The accuracy of the MF-DWRL algorithm can reach 90.57 %, which is about 45 % and 3 % higher than the traditional SVM and RF algorithms, respectively. Meanwhile, compared with the latest DES algorithms DES-MI and Meta-DES, the classification accuracy of the proposed method is still higher. Notably, the MF-DWRS performs the best in the case of classification accuracy among all algorithms. Additionally, the highest kappa value (kappa = 0.89) was attained by the proposed MF-DWRL method, indicating that high consistency and accuracy in classification tasks were achieved. A kappa value close to 1 signifies that there is a high level of agreement among raters and a relatively low error rate. Consequently, it is suggested by this result that the MF-DWRL method is capable of yielding highly consistent results in the classification process and is likely to be considered a preferred classification approach.

Similar to the first experimental, the proposed algorithms MF- DWRL and FS-DWRS perform both better than other methods for the WHU-Hi-LongKou data set. The detailed performance of each algorithm is shown in Table 5, and the thematic maps are described in Fig. 6(a)–(l). The OA of the two proposed can reach 98.66 % and 98.77 %, respectively. Compared with the GBDT algorithm, the MF-

Table 2
The WHU-Hi-LongKou data set.

No.	Samples	Name
1	34511	Corn
2	8374	Cotton
3	3031	Sesame
4	63212	Broad-leaf soybean
5	4151	Narrow-leaf soybean
6	11,854	Rice
7	67056	Water
8	7124	Roads and houses
9	5329	Mixed weed

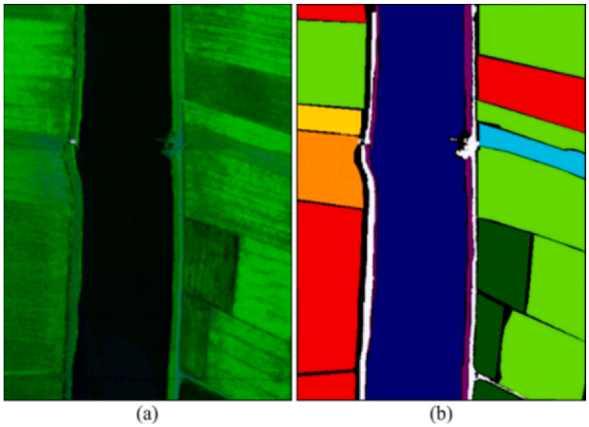

Fig. 3. (a) False-color image and (b) ground truth of theWHU-Hi-LongKou data set.

Table 3
The WHU-Hi-HongHu data set.

No.	Samples	Name
1	14041	Red roof
2	3512	Road
3	21821	Bare soil
4	163285	Cotton
5	6218	Cotton firewood
6	44557	Rape
7	24103	Chinese cabbage
8	4054	Pakchoi
9	10819	Cabbage
10	12394	Tuber mustard
11	11015	Brassica parachinensis
12	8954	Brassica chinensis
13	22507	Small Brassica chinensis
14	7356	Lactuca sativa
15	1002	Celtuce
16	7262	Film covered lettuce
17	3010	Romaine lettuce
18	3217	Carrot
19	8712	White radish
20	3486	Garlic sprout
21	1328	Broad bean
22	4040	Tree

DWRL and FS-DWRS methods perform better. Moreover, compared with three latest ensemble learning algorithms, the two proposed algorithms yield 8 %, 4 %, and 4 % improvements.

For the last data set, the classification performance of all algorithms is shown in Table 6, and the thematic images are shown in Fig. 7(a)–(l). For the third data set, the MF-DWRL and FS-DWRS perform better than other comparative methods. Compared with CRC and ProCRC models, the proposed methods yield 10 % and 13 % improvements, respectively. Moreover, the classification performance of FS-DWRS is better than MF-DWRL.

4. Discussions

4.1. Extendibility of proposed methods

To verify the generalization ability of the proposed algorithm, three sets of classical hyperspectral data are also used for experiments. The overall accuracy (OA), average accuracy (AA), and kappa indexes are used to evaluate the classification of all the comparisons and proposed methods in this section.

According to Table 7, for the Indian Pines data set, the classification performance of proposed methods is better than other comparative models. The accuracy of the MF-DWRL algorithm can reach 89.50 %, which is about 31 % and 3 % higher than the traditional SVM and RF algorithms, respectively. Meanwhile, compared with the classical ensemble learning algorithm GBDT and the latest DES of the proposed method is still higher. Notably, the FS-DWRS performs the best in the case of classification accuracy among all algorithms.

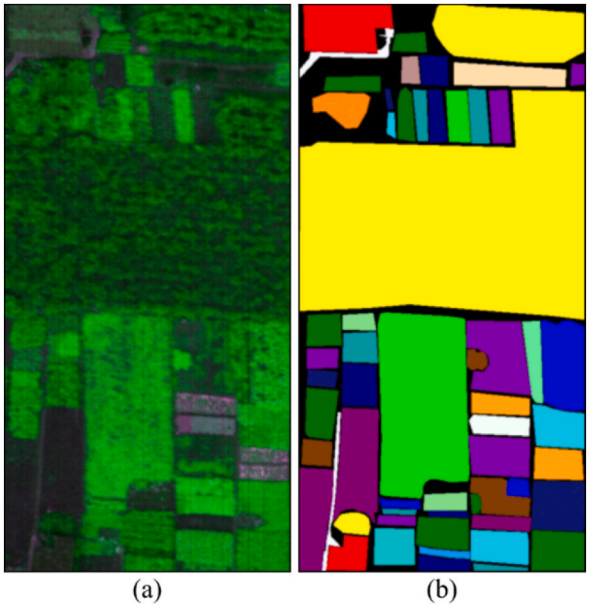

Fig. 4. (a) False-color image and (b) ground truth of the WHU-Hi-HongHu data set.

Table 4
Classification results (%) for the WHU-Hi-HanChuan data set.

Class	SVM	RF	CRC	ProCRC	GBDT	DES-MI	Meta-DES	XGboost	LightGBM	DCNN	MF-DWRL	FS-DWRL
1	33.99	88.39	57.92	32.50	89.93	90.02	85.11	82.55	88.62	86.45	95.35	93.87
2	34.75	71.21	61.47	55.49	69.61	79.36	70.39	68.41	77.04	69.13	71.65	70.82
3	37.53	83.46	68.32	56.24	79.65	85.13	80.95	84.23	89.05	73.43	92.51	95.91
4	69.73	92.70	95.70	94.53	91.38	89.59	91.50	93.83	91.50	92.99	94.34	93.74
5	60.00	99.48	95.65	99.83	95.30	99.39	99.65	94.17	98.35	97.30	99.83	99.83
6	8.28	79.57	68.10	80.33	87.84	83.92	83.45	80.55	76.89	74.01	81.75	84.07
7	79.58	92.86	90.98	81.68	79.38	93.87	92.35	90.48	94.57	92.31	97.18	96.70
8	16.05	82.17	58.24	60.61	77.00	80.10	81.94	85.13	83.15	86.13	80.42	80.28
9	20.04	81.74	58.69	53.59	77.11	77.45	78.46	65.54	80.40	61.86	85.44	83.26
10	40.50	87.48	68.72	88.28	90.67	89.66	89.03	92.14	93.45	92.11	94.82	93.81
11	79.59	96.89	95.80	83.69	83.99	96.70	97.05	91.64	95.10	92.87	98.24	98.46
12	52.07	98.87	88.62	99.53	92.04	97.63	98.76	97.44	98.02	96.31	99.86	99.89
13	23.76	70.83	63.04	48.80	77.13	68.42	75.07	80.00	81.56	68.39	78.91	79.01
14	16.80	93.74	92.31	93.51	89.35	89.52	91.72	93.19	94.43	94.38	93.06	92.17
15	50.83	93.20	87.50	93.47	88.42	90.53	93.11	95.86	97.06	93.84	93.66	92.37
16	65.45	93.52	76.66	98.14	82.13	90.52	94.38	89.39	92.03	89.55	93.84	93.30
OA	45.10	88.04	72.23	72.84	83.01	87.62	87.52	85.29	88.93	85.24	90.57	90.05
AA	43.06	87.88	76.73	76.26	84.43	87.61	87.68	86.54	89.45	85.07	90.68	90.47
Kappa	0.38	0.86	0.68	0.69	0.80	0.86	0.85	0.83	0.87	0.83	0.89	0.88

Similar to the first experimental, the proposed algorithms MF-DWRL and FS-DWRS perform both better than other models for the University of Pavia data set. The OA of the two proposed can reach 94.40 % and 94.17 %, respectively. Moreover, compared with three DES methods, the two proposed algorithms yield 12 %, 11 %, and 11 % improvements (Table 8). Meanwhile, both proposed methods can achieve the highest kappa coefficient value.

For the third data set, the MF-DWRL and FS-DWRS perform better than other comparative methods. Compared with CRC and ProCRC models, the proposed methods yield 5 % and 7 % improvements, respectively. Moreover, the classification performance of FS-DWRS is better than MF-DWRL (Table 9). The proposed method MF-DWRL and FS-DWRS outperforms other comparison algorithms in terms of kappa coefficient performance.

4.2. The effect of different sample sizes

For the three real HSI data set, the number of samples significantly impacts the classification performance. Fig. 8. (a) – (c) show the accuracy of the MF-DWRL and FS-DWRL algorithms when the number of samples changes in range.

For the WHU-Hi-HanChuan data set dataset, the accuracy of the MF-DWRL and FS-DWRL algorithms shows the same trend as the

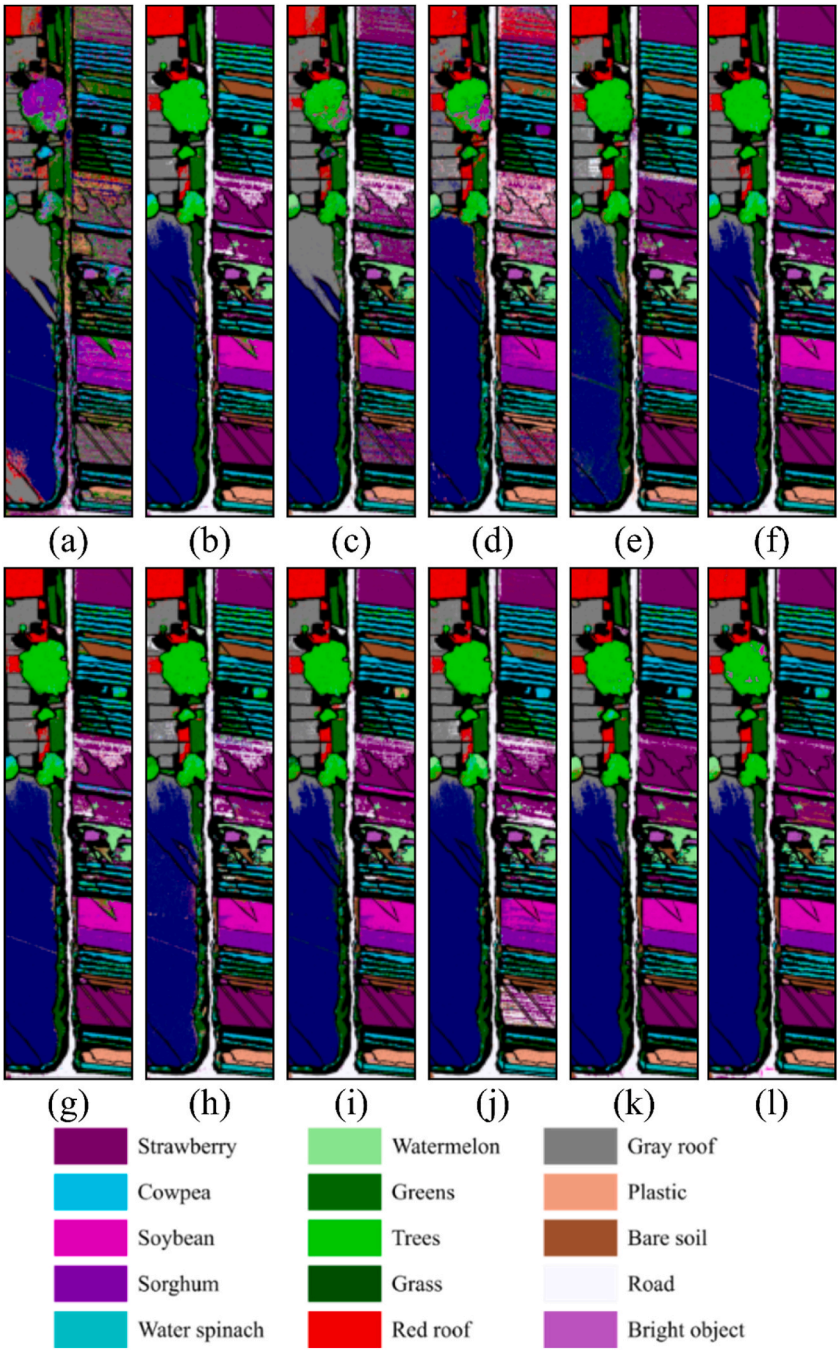

Fig. 5. Classification for the WHU-Hi-LongKou data set. (a) SVM. (b) RF. (c) CRC. (d) ProCRC. (e) GBDT. (f) DES-MI. (g) Meta-DES. (h) XGboost. (i) LightGBM. (j) DCNN. (k)MF-DWRL. (l) FS-DWRL.

sample changes. The best classification accuracy can be obtained when the number of samples is 25. Meanwhile, it can be seen that when the number of samples is from 10 to 20, the classification accuracy of FS-DWRL is higher than MF-DWRL.

For the WHU-Hi-LongKou data set, when the number of samples is 20, the classification accuracy of the two algorithms reaches the highest. However, unlike WHU-Hi-HanChuan data, the classification accuracy of MF-DWRL has always been higher than the FS-DWRL algorithm.

Finally, the classification accuracy of MF-DWRL and FS-DWRL is affected by the number of samples for the WHU-Hi-HongHu data set, similar to the previous two data. Unlike the first two data, the overall classification accuracy of the two algorithms is large, and the classification performance of FS-DWRL is much higher than MF-DWRL.

Table 5
Classification results (%) for the WHU-Hi-LongKou data set.

Class	SVM	RF	CRC	ProCRC	GBDT	DES-MI	Meta-DES	XGboost	LightGBM	DCNN	MF-DWRL	FS-DWRL
1	93.85	96.85	99.49	99.82	96.82	98.22	97.88	97.36	97.58	98.55	98.71	99.49
2	81.61	98.32	98.22	98.24	97.60	98.61	98.26	98.79	98.38	95.11	99.08	99.05
3	84.99	98.03	99.63	99.93	93.08	97.69	97.86	93.08	97.19	99.83	98.66	99.03
4	54.99	88.12	84.93	71.09	87.77	90.70	85.62	90.38	93.11	93.97	97.38	97.32
5	75.12	97.91	99.56	99.42	95.14	96.59	96.94	96.57	96.42	99.34	98.95	99.15
6	90.39	83.99	91.53	87.99	86.08	85.38	89.47	78.49	92.18	98.73	99.14	99.17
7	99.88	99.97	99.99	100.00	99.92	99.94	99.96	99.14	99.95	99.89	99.96	99.94
8	62.48	93.65	91.13	83.46	83.89	88.14	91.46	95.02	95.16	97.92	97.92	98.07
9	56.65	87.21	93.14	74.01	81.85	75.70	74.91	86.90	82.99	95.13	96.11	95.61
OA	80.57	94.17	94.19	89.01	93.53	94.77	93.47	94.33	96.21	97.37	98.66	98.77
AA	77.77	93.78	95.29	90.44	91.35	92.33	92.48	92.86	94.77	97.61	98.43	98.54
Kappa	0.76	0.92	0.92	0.86	0.92	0.93	0.92	0.93	0.95	0.97	0.98	0.98

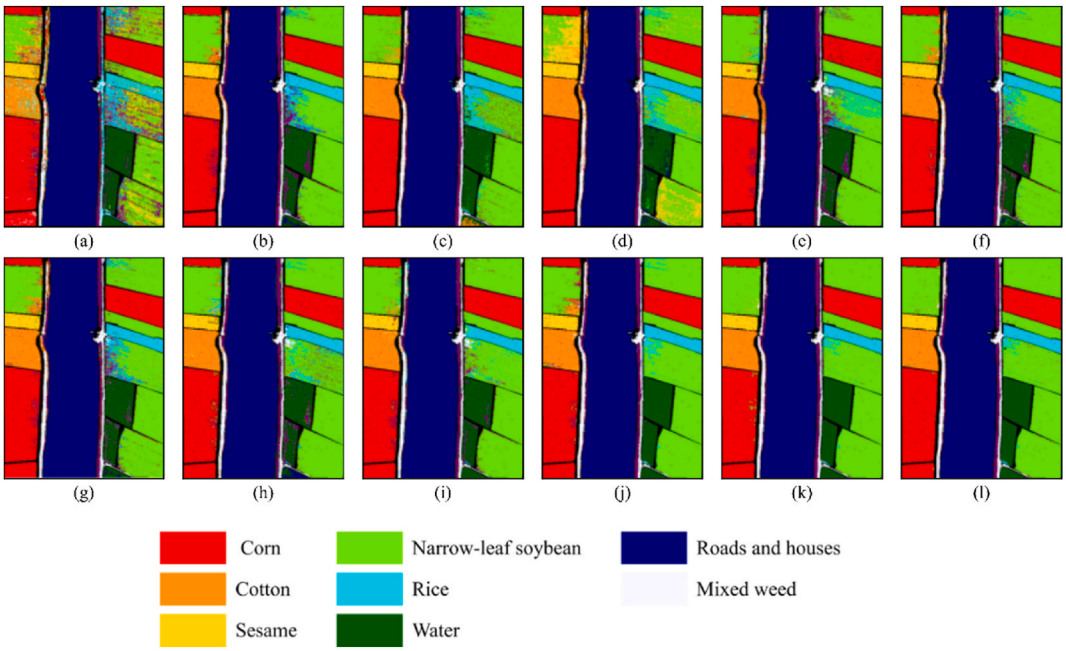

Fig. 6. Classification for the WHU-Hi-HongHu data set. (a) SVM. (b) RF. (c) CRC. (d) ProCRC. (e) GBDT. (f) DES-MI. (g) Meta-DES. (h) XGboost. (i) LightGBM. (j) DCNN. (k)MF-DWRL. (l) FS-DWRL.

4.3. Parameters analysis for number of λ

Fig. 9 shows the effects of parameter λ on the classification accuracy. For WHU-Hi-HanChuan data (Fig. 9(a)), the classification accuracy of MF-DWRL increases with the gradual decrease in regularization parameter λ. The classification accuracy of MF-DWRL and FS-DWRL is increasing first, and then the overall classification performance should be due to MF-DWRL. For theWHU-Hi-LongKou data (Fig. 9(b)), as the parameter λ decreases, the classification accuracy of the MF-DWRL algorithm is increases. For FS-DWRL, the classification accuracy rises first and then drops. When λ is 1e-3, both algorithms reach the highest accuracy.

The classification performance of WHU-Hi-HongHu data (Fig. 9(c)) has gradually increased with the decrease when regularization parameter λ in range 1e-1 and 1e-3. When λ is 1e-3, both algorithms reach the highest accuracy.

*4.4. Parameters analysis for number of bootstrap iterations **n_r***

For the FS-DWRL algorithm, the paper discusses the impact of the number of resamples times on the classification accuracy (Fig. 10). It can be seen from Fig. 10(a)–(c) that the number of resample times has little effect on the classification accuracy of the proposed method. Meanwhile, with the increase of the number of resample times, the classification accuracy has decreased first and then increased. It is worth noting that for three different hyperspectral data, when the parameter is set as 10, the classification accuracy reaches the highest. In summary, the model is not sensitive to the change of parameter, and has great generalization and robustness.

Table 6
Classification results (%) for the WHU-Hi-HongHu dataset.

Class	SVM	RF	CRC	ProCRC	GBDT	DES-MI	Meta-DES	XGboost	LightGBM	DCNN	MF-DWRL	FS-DWRL
1	66.89	92.37	72.45	89.84	88.75	95.51	94.10	88.21	89.29	92.00	97.08	97.28
2	50.06	90.67	92.69	91.74	89.63	89.14	89.37	89.43	89.51	92.26	94.74	94.86
3	70.21	84.67	86.90	83.16	82.32	86.47	85.58	84.50	84.12	82.99	85.12	85.44
4	58.95	96.70	91.47	82.89	90.44	96.52	96.91	92.81	96.93	89.90	96.78	97.41
5	30.50	96.40	83.35	84.65	92.09	92.64	93.30	97.13	96.92	91.94	95.98	96.81
6	77.14	89.30	92.56	92.64	90.27	90.32	89.48	89.58	88.82	88.79	92.42	91.11
7	18.96	64.74	43.96	43.19	59.15	67.52	65.28	60.06	62.40	67.64	62.52	58.17
8	8.37	91.28	77.97	82.49	92.11	86.51	83.47	98.78	99.58	84.52	95.63	97.80
9	79.07	94.64	92.96	96.00	92.65	93.00	92.74	92.18	92.49	91.22	92.72	92.13
10	29.16	79.49	65.57	53.47	71.95	77.20	74.28	85.97	87.31	75.43	85.21	89.28
11	34.84	60.28	54.80	47.44	79.04	64.33	59.17	73.23	78.85	60.73	80.67	81.04
12	34.27	83.85	67.77	71.97	85.42	80.69	77.59	89.22	90.86	85.68	90.35	92.49
13	48.02	77.82	34.37	33.57	66.99	76.11	74.95	72.77	74.67	68.61	82.83	84.69
14	43.54	81.60	65.07	69.60	84.38	76.02	79.14	83.73	85.89	84.01	87.09	87.89
15	58.55	95.17	91.19	95.59	91.92	94.54	94.65	95.70	95.80	95.49	97.06	94.75
16	48.13	98.43	99.49	99.81	99.71	97.99	99.00	99.72	99.72	97.09	99.64	99.75
17	65.81	90.24	93.95	94.80	91.79	85.20	89.59	91.79	91.79	90.88	93.31	93.72
18	37.09	91.79	91.76	86.14	85.70	87.37	87.44	86.36	86.77	95.01	94.44	94.73
19	26.09	73.54	66.10	62.31	76.85	66.17	70.63	78.35	80.24	79.47	76.04	72.28
20	45.87	94.62	92.99	88.01	90.13	88.97	93.36	90.83	95.34	97.50	99.04	99.04
21	73.98	95.86	99.30	94.69	98.75	93.75	97.81	98.28	99.14	100.00	99.61	99.69
22	44.21	99.12	99.00	98.67	97.44	96.59	97.87	98.27	98.45	97.37	98.95	98.97
OA	54.56	89.00	80.94	77.20	85.48	88.69	88.39	87.45	89.77	85.51	90.96	91.08
AA	47.71	87.39	79.80	79.21	86.25	85.57	85.71	88.04	89.31	86.75	90.78	90.88
Kappa	0.47	0.86	0.76	0.72	0.82	0.86	0.85	0.84	0.87	0.82	0.89	0.89

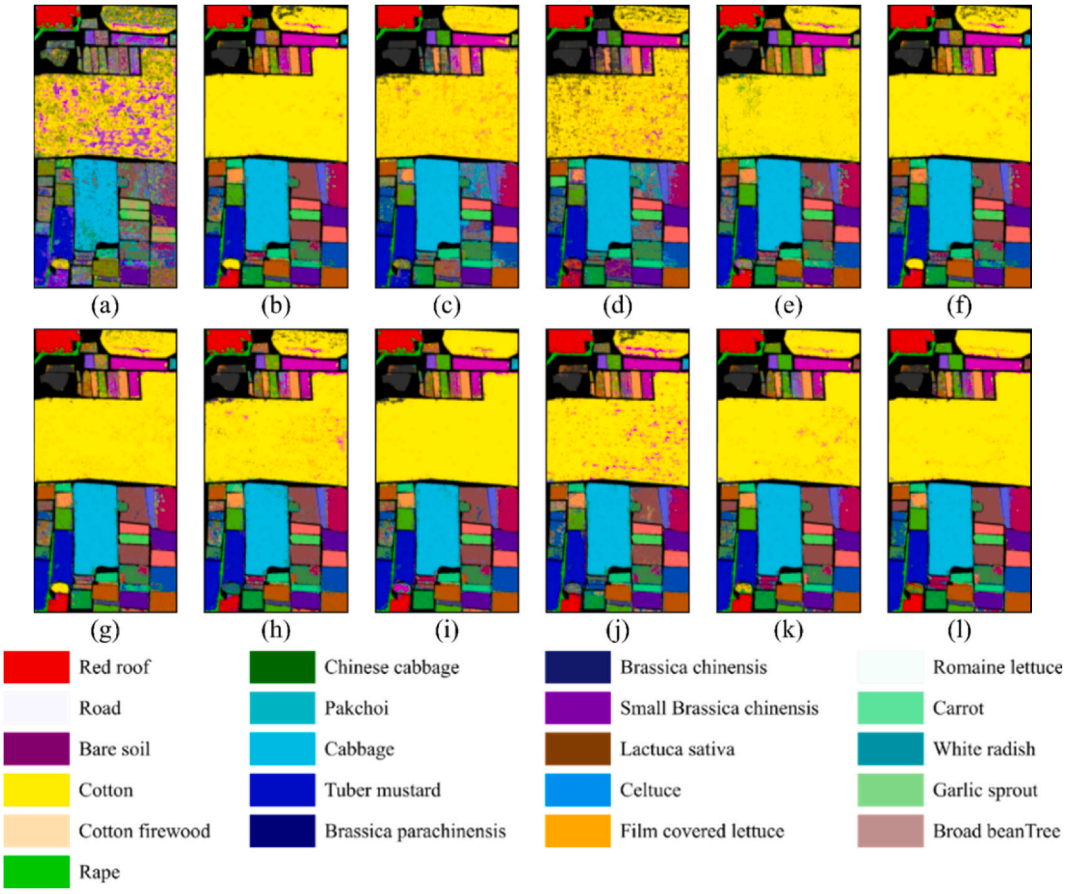

Fig. 7. Classification accuracy of three data set versus varying samples of proposed methods. (a) SVM. (b) RF. (c) CRC. (d) ProCRC. (e) GBDT. (f) DES-MI. (g) Meta-DES. (h) XGboost. (i) LightGBM. (j) DCNN. (k)MF-DWRL. (l) FS-DWRL.

Table 7
Classification results (%) for the Indian Pines data set.

Class	SVM	RF	CRC	ProCRC	GBDT	DES-MI	Meta-DES	XGboost	LightGBM	DCNN	MF-DWRL	FS-DWRL
1	94.12	100.00	100.00	100.00	88.24	100.00	100.00	100.00	100.00	93.75	100.00	100.00
2	20.36	69.86	69.35	72.23	76.69	79.86	77.99	76.33	73.02	77.00	78.99	78.49
3	34.39	77.24	77.62	79.27	84.07	87.23	86.09	81.16	84.45	86.28	82.81	82.68
4	44.50	93.50	80.50	88.00	80.00	94.50	94.00	98.00	99.50	71.50	98.00	98.50
5	63.60	82.02	88.99	88.54	75.28	88.54	86.29	82.47	82.92	85.98	89.89	90.56
6	74.20	94.06	95.80	93.91	90.14	96.96	97.25	91.01	93.19	94.44	94.93	95.07
7	100.00	100.00	100.00	100.00	83.33	100.00	100.00	83.33	100.00	100.00	100.00	100.00
8	100.00	100.00	100.00	100.00	99.55	100.00	100.00	100.00	100.00	100.00	100.00	100.00
9	100.00	100.00	100.00	100.00	100.00	100.00	100.00	100.00	100.00	100.00	100.00	100.00
10	73.55	79.01	84.80	86.83	80.09	76.23	82.23	70.99	77.52	85.61	82.66	82.01
11	66.14	79.06	85.31	88.41	82.24	76.86	80.88	84.81	82.57	75.47	90.73	90.60
12	34.71	72.12	79.50	81.65	82.37	60.43	70.50	90.11	86.87	77.02	81.12	80.04
13	93.45	96.43	97.62	99.40	86.90	95.24	96.43	95.24	97.62	98.75	97.62	97.62
14	78.12	94.45	99.67	100.00	93.47	91.18	97.22	99.02	99.18	98.60	99.76	99.76
15	40.35	88.76	91.35	85.88	95.68	75.50	89.63	96.54	96.83	96.17	97.98	97.98
16	93.44	100.00	100.00	100.00	100.00	100.00	98.36	100.00	100.00	100.00	100.00	98.36
OA	58.76	82.43	85.87	87.39	84.49	82.81	85.79	86.09	86.06	84.74	89.50	89.69
AA	69.43	89.16	90.66	91.51	87.38	88.91	91.05	90.56	92.10	90.03	93.40	93.23
Kappa	0.54	0.80	0.84	0.86	0.82	0.80	0.84	0.84	0.84	0.83	0.88	0.88

Table 8
Classification results (%) for the University of Pavia data set.

Class	SVM	RF	CRC	ProCRC	GBDT	DES-MI	Meta-DES	XGboost	LightGBM	DCNN	MF-DWRL	FS-DWRL
1	50.43	72.39	86.07	81.89	75.59	88.66	87.63	90.24	91.06	96.95	96.24	92.60
2	57.19	73.83	92.36	84.42	61.59	81.34	79.38	77.99	70.12	89.94	90.20	93.01
3	66.19	76.62	88.70	96.49	77.59	87.21	81.14	88.70	90.28	83.16	83.13	89.27
4	67.94	87.94	95.73	95.80	64.62	83.61	92.18	71.09	78.19	98.91	97.56	97.73
5	86.43	99.25	99.77	100.00	92.84	96.15	99.40	93.74	93.74	99.92	100.00	100.00
6	50.35	80.95	91.14	91.99	86.30	71.09	76.56	93.09	70.85	99.48	97.76	97.30
7	83.89	97.86	98.55	99.24	92.98	95.95	98.24	98.09	97.94	100.00	99.54	98.93
8	60.46	76.27	88.72	46.86	80.31	71.41	78.62	79.00	86.16	99.23	96.60	95.77
9	98.49	99.78	98.81	99.89	85.13	95.69	100.00	79.42	91.92	100.00	99.89	100.00
OA	59.45	77.90	91.55	84.37	71.72	82.09	82.92	82.92	78.46	94.08	94.40	94.17
AA	69.04	84.99	93.32	88.51	79.66	85.68	88.13	85.71	85.58	96.40	96.07	96.58
Kappa	0.50	0.72	0.89	0.80	0.65	0.77	0.78	0.78	0.73	0.92	0.93	0.92

Table 9
Classification results (%) for the Salinas data set.

Class	SVM	RF	CRC	ProCRC	GBDT	DES-MI	Meta-DES	XGboost	LightGBM	DCNN	MF-DWRL	FS-DWRL
1	80.04	99.90	99.80	100.00	89.44	100.00	99.70	94.10	92.25	100.00	100.00	100.00
2	56.22	100.00	99.81	99.95	95.24	98.01	99.68	99.76	99.89	99.62	99.95	100.00
3	63.38	92.12	99.49	93.34	95.07	99.03	93.13	80.32	92.22	92.37	99.79	99.80
4	52.60	98.70	96.68	98.12	98.70	97.11	90.03	96.46	99.28	99.70	99.70	99.13
5	73.80	91.45	91.83	92.43	61.99	90.55	92.99	81.71	86.88	98.48	97.69	97.34
6	90.15	99.14	99.29	99.85	86.60	98.89	98.35	95.09	91.16	99.97	99.85	98.61
7	85.91	99.75	98.40	99.92	96.05	97.65	99.36	99.47	99.72	99.91	99.80	99.89
8	51.59	68.49	61.08	49.41	63.70	94.41	90.65	97.62	93.88	51.71	90.02	71.27
9	91.25	96.84	99.19	98.05	88.28	95.01	96.80	79.41	88.68	99.72	99.98	99.98
10	55.23	88.95	92.35	94.86	91.52	77.91	86.57	86.02	88.68	98.76	98.58	95.26
11	59.36	88.75	95.94	97.35	77.98	87.43	88.75	74.67	75.14	93.42	99.81	94.33
12	16.95	90.82	87.85	94.73	17.79	87.79	93.90	79.92	84.19	100.00	100.00	100.00
13	72.08	97.79	90.40	92.60	97.90	94.92	98.01	98.68	98.45	99.54	97.83	98.23
14	33.30	93.40	92.45	90.00	33.96	66.04	90.09	87.26	90.38	92.07	99.13	94.43
15	54.22	70.46	65.21	67.31	69.04	40.71	45.95	69.14	60.47	87.20	87.30	78.15
16	85.92	97.72	98.72	100.00	92.32	89.71	95.27	99.44	100.00	100.00	98.64	99.00
OA	64.78	86.81	85.10	83.27	77.41	86.23	87.73	88.30	88.25	87.32	90.22	93.24
AA	63.87	92.14	91.78	91.74	78.47	88.45	91.20	88.69	90.08	95.53	95.34	96.53
Kappa	0.61	0.85	0.83	0.81	0.75	0.85	0.86	0.87	0.87	0.86	0.89	0.92

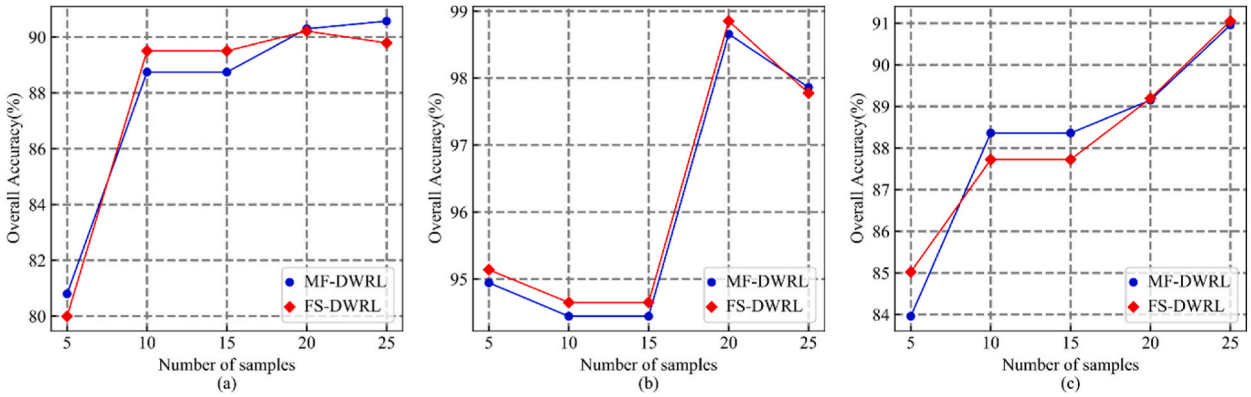

Fig. 8. Classification accuracy versus varying λ of proposed methods. (a) Han Chuan data set. (b) Long Kou data set. (c) Hong Hu data set.

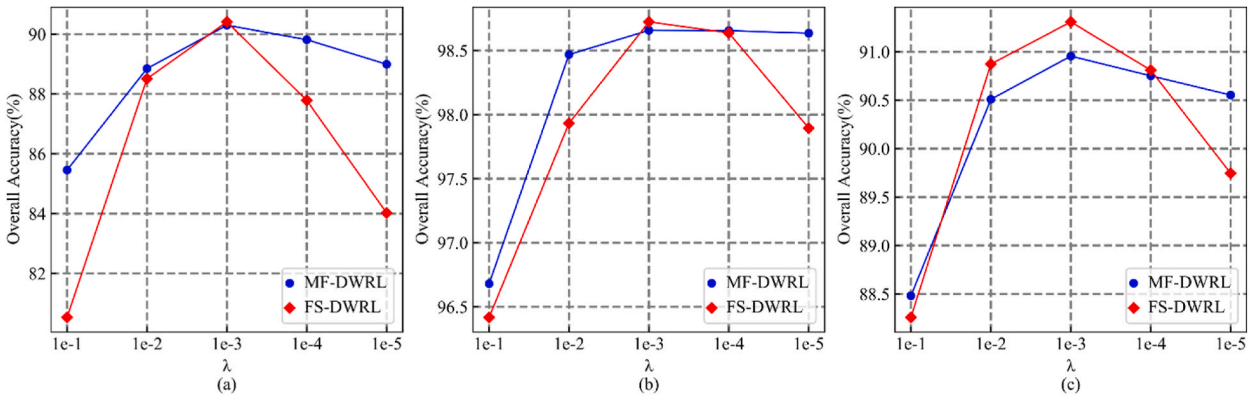

Fig. 9. Classification accuracy versus varying λ of proposed methods. (a) Han Chuan data set. (b) Long Kou data set. (c) Hong Hu data set.

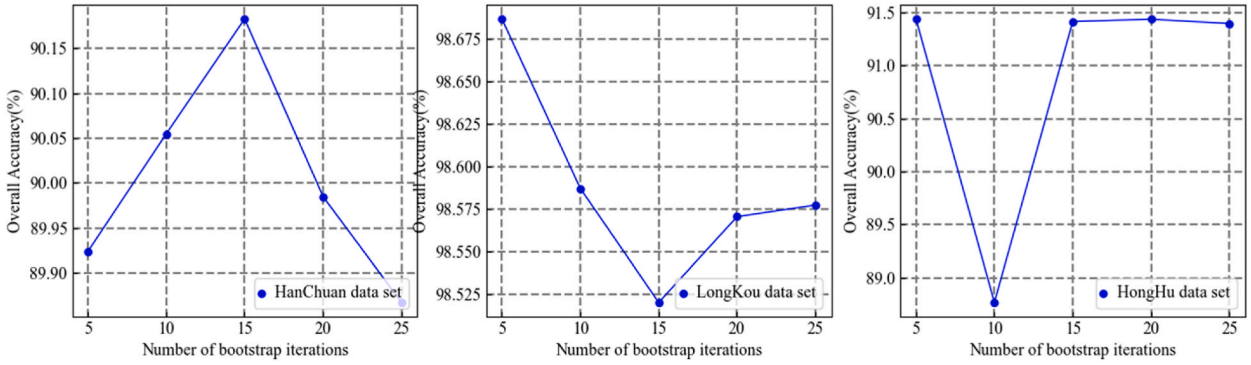

Fig. 10. Classification accuracy versus varying number of bootstrap iterations of proposed methods. (a) Han Chuan data set. (b) Long Kou data set. (c) Hong Hu data set.

Table 10
Classification results (%) for the three data sets based on different feature combinations.

	S	E	G	SE	SG	EG)	SEG	MF-DWRL	FS-DWRL
Han Chuan	59.57	85.19	35.73	85.10	44.24	57.73	60.00	90.57	90.05
Long Kou	89.94	98.56	47.10	98.23	63.82	82.98	84.44	98.66	98.77
Hong Hu	60.50	91.44	8.04	89.12	33.59	55.58	57.14	90.96	91.08

4.5. Analysis of feature selection

Table 10 demonstrates the classification results for three groups using different datasets. Here, S, E, G represent spectral features, emp features, and Gabor features respectively, while SE, SG, EG, SEG denote different combinations of features. The last two methods incorporate a feature selection process. A paragraph of analysis indicates the advantages of the proposed methods. Based on the provided data, it can be observed that the proposed methods (MF-DWRL and FS-DWRL) achieve the highest classification accuracies across all combinations. This suggests that the proposed methods can effectively enhance classification performance when dealing with different feature combinations. Specifically, the classification accuracies of MF-DWRL and FS-DWRL methods are consistently higher than those of other methods across all feature combinations (S, E, G, SE, SG, EG, SEG). This indicates that these two methods not only fully utilize the information from individual features but also demonstrate stronger classification capabilities in feature combinations. In contrast, other methods may perform poorly in certain feature combinations, possibly due to differences in feature correlation or importance. Furthermore, the most prominent among these methods is FS-DWRL, with classification accuracies approaching or exceeding 98 % in most feature combinations. This suggests that FS-DWRL excels in feature selection, extracting the most representative features from the original set and significantly improving classification accuracy. In conclusion, the proposed methods demonstrate excellent performance across multiple feature combinations, with FS-DWRL particularly standing out for its superior feature selection capabilities, making it a highly promising classification approach.

5. Conclusion

In conclusion, this paper introduces a novel dynamic ensemble weighted residuals (DES) learning framework designed to integrate prior classification information and achieve superior classification performance. The DES framework presents an innovative approach for the weighted selection and fusion of multiple features, utilizing the DES methodology to acquire prior classification insights for various features within the region of competence (RoC). This prior information is effectively harnessed to constrain the residuals of each classifier, thereby enhancing overall classification accuracy.

Furthermore, the DES framework incorporates the bootstrap method for resampling the training set, thereby generating a diverse pool of classifiers. By leveraging the prior classification behavior of each classifier within the RoC, the DES framework derives weighted residual fusion outcomes for different samples. In contrast to conventional ensemble learning techniques and DES methods, the proposed framework dynamically selects both features and samples, which significantly improves classification performance.

Empirical evaluations substantiate the superiority of the proposed DES framework over existing models, demonstrating markedly improved classification accuracy. Additionally, the DES framework exhibits robustness to parameter variations, thereby mitigating the need for intricate parameter tuning in practical applications. The efficacy of the proposed methods is further corroborated by classification results obtained from three hyperspectral image (HSI) datasets.

Looking ahead, several promising avenues for future research are apparent. First, extending the DES framework to domains beyond image classification—such as natural language processing, time series analysis, and biomedical data analysis—represents an intriguing direction. Second, exploring the application of the DES framework to diverse remote sensing tasks, including object detection, land cover mapping, and change detection, holds considerable potential. Furthermore, the integration of advanced techniques, such as deep learning-based approaches and online learning strategies, could further augment the performance of the DES framework.

In summary, the proposed dynamic ensemble weighted residuals learning framework offers a robust methodology for incorporating prior classification information and achieving enhanced classification outcomes. This research provides valuable insights into the field of machine learning and remote sensing analysis, setting the stage for future advancements in ensemble learning methodologies.

Data availability

Data will be made available on request.

Funding

This research was funded by the Fund of National Sensor Network Engineering Technology Research Center (No. NSNC202103).

CRediT authorship contribution statement

Jing Wang: Writing – original draft, Software, Data curation. **Guoguo Yang:** Supervision, Investigation, Formal analysis, Conceptualization. **Hongliang Lu:** Writing – review & editing, Supervision, Methodology, Formal analysis, Conceptualization.

Declaration of competing interest

The authors declare that they have no known competing financial interests or personal relationships that could have appeared to influence the work reported in this paper.

Acknowledgments

The authors would like to thank Prof. Y. Zhong at the Wuhan University, for providing WHU-Hi hyperspectral data sets, Prof. P. Gamba at the University of Pavia, Pavia, Italy, for providing the ROSIS data and Prof. D. Landgrebe from Purdue University for providing the AVIRIS image of Indian Pines and Salinas valley.

References

[1] D. Landgrebe, Hyperspectral image data analysis, IEEE Signal Process. Mag. 19 (2022) 17–28.
[2] H. Su, Z. Wu, H. Zhang, Q. Du, Hyperspectral anomaly detection: a survey, IEEE Geosci. Remote Sens. Mag. 10 (2022) 64–90.
[3] H. Su, C. Jia, P. Zheng, Q. Du, Superpixel-based weighted collaborative sparse regression and reweighted low-rank representation for hyperspectral image unmixing, IEEE J. Sel. Top. Appl. Earth Obs. Rem. Sens. 15 (2022) 393–408.
[4] H. Chen, et al., Automatic live and dead cell classification via hyperspectral imaging. 2019 10th workshop on hyperspectral imaging and signal processing, Evolution in Remote Sensing (WHISPERS) (2019) 1–5.
[5] C.M. Gevaert, J. Suomalainen, J. Tang, L. Kooistra, Generation of spectral–temporal response surfaces by combining multispectral satellite and hyperspectral UAV imagery for precision agriculture applications. IEEE J. Sel. Topics appl. Earth observ, Rem. Sens. 8 (2015) 3140–3146.
[6] T.J. Cudahy, L.B. Whitbourn, P.M. Connor, P. Mason, R.N. Phillips, Mapping surface mineralogy and scattering behavior using backscattered reflectance from a hyperspectral midinfrared airborne CO/sub 2/laser system (MIRACO/sub 2/LAS), IEEE Trans. Geosci. Rem. Sens. 37 (1999) 2019–2034.
[7] S. Kendler, I. Ron, S. Cohen, R. Raich, Z. Mano, B. Fishbain, Detection and identification of sub-millimeter f ilms of organic compounds on environmental surfaces using short-wave infrared hyperspectral imaging: algorithm development using a synthetic set of targets, IEEE Sensor. J. 19 (2019) 2657–2664.
[8] B. Tu, C. Zhou, X. Liao, Q. Li, Y. Peng, Feature extraction via 3-D block characteristics sharing for hyperspectral image classification, IEEE Trans. Geosci. Rem. Sens. 59 (2021) 10503–10518.
[9] Z. Wu, et al., Scheduling-guided automatic processing of massive hyperspectral image classification on cloud computing architectures, IEEE Trans. Cybern. 51 (2021) 3588–3601.
[10] Z. Gao, L. Tong, J. Zhou, B. Qian, J. Yu, C. Xiao, Stochastic depth residual network for hyperspectral image classification, IEEE Trans. Geosci. Rem. Sens. 60 (2022) 1–13.
[11] C. Yu, et al., Hyperspectral image classification method based on CNN architecture embedding with hashing semantic feature, IEEE J. Sel. Top. Appl. Earth Obs. Rem. Sens. 12 (2019) 1866–1881.
[12] S. Zhong, et al., Class feature weighted hyperspectral image classification, IEEE J. Sel. Top. Appl. Earth Obs. Rem. Sens. 12 (2019) 4728–4745.
[13] H. Su, B. Zhao, Q. Du, P. Du, Z. Xue, Multifeature dictionary learning for collaborative representation classification of hyperspectral imagery, IEEE Trans. Geosci. Rem. Sens. 56 (2017) 2467–2484.
[14] H. Su, W. Yao, Z. Wu, P. Zheng, Q. Du, Kernel low-rank representation with elastic net for China coastal wetland land cover classification using GF-5 hyperspectral imagery, ISPRS J. Photogrammetry Remote Sens. 171 (2021) 238–252.
[15] G. Wang, P. Ren, Hyperspectral image classification with feature-oriented adversarial active learning, Rem. Sens. 12 (2020) 3879, https://doi.org/10.3390/rs12233879.
[16] C. Zhao, Y. Yuan, B. Zhang, M. Li, Ionosphere sensing with a low-cost, single-frequency, multi-GNSS receiver, IEEE Trans. Geosci. Rem. Sens. 57 (2) (Feb. 2019) 881–892, https://doi.org/10.1109/TGRS.2018.2862623.
[17] C. Yu, R. Han, M. Song, C. Liu, C.-I. Chang, Feedback attention-based dense CNN for hyperspectral image classification, IEEE Trans. Geosci. Rem. Sens. 60 (2022) 1–16, https://doi.org/10.1109/TGRS.2021.3058549. Art no. 5501916.
[18] M. Xu, Q. Zhao, S. Jia, Multiview spatial–spectral active learning for hyperspectral image classification, IEEE Trans. Geosci. Rem. Sens. 60 (2022) 1–15, https://doi.org/10.1109/TGRS.2021.3095292. Art no. 5512415.
[19] Z. Ye, T. Sun, S. Shi, L. Bai, J.E. Fowler, Local–global active learning based on a graph convolutional network for semi-supervised classification of hyperspectral imagery, Geosci. Rem. Sens. Lett. IEEE 20 (2023) 1–5, https://doi.org/10.1109/LGRS.2023.3244758. Art no. 5501805.
[20] C. Zhao, et al., Hyperspectral image classification with multi-attention transformer and adaptive superpixel segmentation-based active learning, IEEE Trans. Image Process. 32 (2023) 3606–3621, https://doi.org/10.1109/TIP.2023.3287738.
[21] L. Zhao, W. Luo, Q. Liao, S. Chen, J. Wu, Hyperspectral image classification with contrastive self-supervised learning under limited labeled samples, Geosci. Rem. Sens. Lett. IEEE 19 (2022) 1–5, https://doi.org/10.1109/LGRS.2022.3159549. Art no. 6008205.
[22] Z. Zhu, Z. Wang, D. Li, Y. Zhu, W. Du, Geometric structural ensemble learning for imbalanced problems, IEEE Trans. Cybern. 50 (2020) 1617–1629.
[23] G. Fumera, F. Roli, A. Serrau, A theoretical analysis of bagging as a linear combination of classifiers, IEEE Trans. Pattern Anal. Mach. Intell. 30 (2008) 1293–1299.
[24] G. Martínez-Muñoz, D. Hernández-Lobato, A. Suárez, An analysis of ensemble pruning techniques based on ordered aggregation, IEEE Trans. Pattern Anal. Mach. Intell. 31 (2009) 245–259.
[25] T.M. Khoshgoftaar, J. Van Hulse, A. Napolitano, Comparing boosting and bagging techniques with noisy and imbalanced data, IEEE Trans. Syst. Man Cybern. Syst. Hum. 41 (2011) 552–568.
[26] M. Chen, Y. Yang, P.C. Loh, F. Blaabjerg, A single-source nine-level boost inverter with a low switch count, IEEE Trans. Ind. Electron. 69 (2022) 2644–2658.
[27] M. Veerachary, M.R. Khuntia, Design and analysis of two-switch-based enhanced gain buck–boost converters, IEEE Trans. Ind. Electron. 69 (2022) 3577–3587.
[28] R. Barzegarkhoo, M. Farhangi, R.P. Aguilera, Y.P. Siwakoti, S.S. Lee, Switched-boost common-ground five-level (SBCG5L) grid-connected inverter with single-stage dynamic voltage boosting concept, in: 2021 IEEE Energy Conversion Congress and Exposition (ECCE), 2021, pp. 1014–1019.
[29] E. Zhang, X. Zhang, L. Jiao, L. Li, B. Hou, Spectral–spatial hyperspectral image ensemble classification via joint sparse representation, Pattern Recogn. 59 (2016) 42–54.
[30] Z. Li, F. Xiong, J. Zhou, J. Wang, J. Lu, Y. Qian, BAE-Net: a band attention aware ensemble network for hyperspectral object tracking, in: 2020 IEEE International Conference on Image Processing (ICIP), 2020.
[31] H. Su, Y. Yu, Q. Du, P. Du, Ensemble learning for hyperspectral image classification using tangent collaborative representation, IEEE Trans. Geosci. Rem. Sens. 58 (2020) 3778–3790.
[32] R.M.O. Cruz, H.H. Zakane, R. Sabourin, G.D.C. Cavalcanti, Dynamic ensemble selection VS K-NN: why and when dynamic selection obtains higher classification performance?, in: Proc. 7th Int. Conf. Image Process. Theory, Tools Appl. IPTA 2017, 2018. Janua).
[33] R.M.O. Cruz, M.A. Souza, R. Sabourin, G.D.C. Cavalcanti, Dynamic ensemble selection and data preprocessing for multi-class imbalance learning, Int. J. Pattern Recogn. Artif. Intell. 33 (2019) 1940009.
[34] H.R. Ko, R. Sabourin, A.S. Britto, From dynamic classifier selection to dynamic ensemble selection, Pattern Recogn. 41 (2008) 1718–1731.
[35] R.M.O. Cruz, R. Sabourin, G.D.C. Cavalcanti, Dynamic classifier selection: recent advances and perspectives, Inf. Fusion 41 (2018) 195–216.
[36] R.A.S. Albuquerque, A.F.J. Costa, E. Miranda Dos Santos, R. Sabourin, R. Giusti, A decision-based dynamic ensemble selection method for concept drift, Proc. - Int. Conf. Tools with Artif. Intell. ICTAI. (2019) 1132–1139.
[37] L.P. Cavalheiro, J.P. Barddal, A. de S. Britto, L. Heutte, scikit-dyn2sel – A dynamic selection framework for data streams, Arxiv (2020), 1–5.
[38] T. Woloszynski, M. Kurzynski, A probabilistic model of classifier competence for dynamic ensemble selection, Pattern Recogn. 44 (2011) 2656–2668.
[39] B.B. Damodaran, R.R. Nidamanuri, Y. Tarabalka, Dynamic ensemble selection approach for hyperspectral image classification with joint spectral and spatial information, IEEE J. Sel. Top. Appl. Earth Obs. Rem. Sens. 8 (2015) 2405–2417.

[40] B.B. Damodaran, R.R. Nidamanuri, Dynamic linear classifier system for hyperspectral image classification for land cover mapping, IEEE J. Sel. Top. Appl. Earth Obs. Rem. Sens. 7 (2014) 2080–2093.
[41] H. Lu, H. Su, J. Hu, Q. Du, Dynamic ensemble learning with multi-view kernel collaborative subspace clustering for hyperspectral image classification, IEEE J. Sel. Top. Appl. Earth Obs. Rem. Sens. 5 (2022) 681–2695.
[42] H. Su, W. Yao, Z. Wu, P. Zheng, Q. Du, Kernel low-rank representation with elastic net for China coastal wetland land cover classification using GF-5 hyperspectral imagery, ISPRS J. Photogrammetry Remote Sens. 171 (2020) 238–252.
[43] H. Su, Y. Hu, H. Lu, W. Sun, Q. Du, Diversity-driven multikernel collaborative representation ensemble for hyperspectral image classification, IEEE J. Sel. Top. Appl. Earth Obs. Rem. Sens. 15 (2022) 2861–2876.
[44] H. Su, Y. Yu, Z. Wu, Q. Du, Random subspace-based k-nearest class collaborative representation for hyperspectral image classification, IEEE Trans. Geosci. Rem. Sens. 59 (2021) 6840–6853.
[45] H. Su, B. Zhao, Q. Du, P. Du, Kernel collaborative representation with local correlation features for hyperspectral image classification, IEEE Trans. Geosci. Rem. Sens. 57 (2019) 1230–1241.
[46] Y. Zhong, X. Hu, C. Luo, X. Wang, J. Zhao, L. Zhang, WHU-Hi: UAV-borne hyperspectral with high spatial resolution (H2) benchmark datasets and classifier for precise crop identification based on deep convolutional neural network with CRF, Remote Sens. Environ. 250 (2020) 112012.
[47] S. Liu, Y. Cui, Y. Ma, P. Liu, Short-term load forecasting based on GBDT combinatorial optimization. 2018 2nd IEEE Conference on Energy Internet and Energy System Integration (EI2), 2018, pp. 1–5.
[48] X. Sun, L. Guo, W. Zhang, Z. Wang, Q. Yu, Small aerial target detection for airborne infrared detection systems using LightGBM and trajectory constraints, IEEE J. Sel. Top. Appl. Earth Obs. Rem. Sens. 14 (2021) 9959–9973.
[49] P. Liu, B. Fu, S.X. Yang, L. Deng, X. Zhong, H. Zheng, Optimizing survival analysis of XGBoost for ties to predict disease progression of breast cancer, IEEE Trans. Biomed. Eng. 68 (2021) 148–160.
[50] S. García, Z.L. Zhang, A. Altalhi, S. Alshomrani, F. Herrera, Dynamic ensemble selection for multi-class imbalanced datasets, Inf. Sci. (2018) 445–446.
[51] R.M.O. Cruz, R. Sabourin, G.D.C. Cavalcanti, Dynamic classifier selection: recent advances and perspectives, Inf. Fusion 41 (2018) 195–216.